Int. J. Electrochem. Sci., 13 **(2018)** 1985 – 2000, doi: 10.20964/2018.02.61

International Journal of
ELECTROCHEMICAL
SCIENCE
www.electrochemsci.org

Experimental and Theoretical Calculations on Corrosion Inhibition of Bronze in 0.5 M HCl by Some Schiff Bases

Zhe Zhang [1], *Le Ruan*[1 *], *Weipeng Zhang* [1], *Yuzeng Lyu* [2], *Wei Shang* [1], *Yuqing Wen* [1], *Xiuying Li*[1], *Ling Wu* [3],*Yanni Jiao* [4]

[1] Guangxi Key Laboratory of Electrochemical and Magneto-chemical Functional Materials, College of Chemistry and Bioengineering, Guilin University of Technology, Guilin 541004, PR China
[2] Engineering Research Center of Exploration for hidden Nonferrous and Precious Metal Ore Deposits, Ministry of Education, 541004, PR China
[3] School of Chemistry and Chemical Engineering, Shandong University, Jinan 250100, PR China
[4] Shandong Center for Disease Control and Prevention, Jinan 250014, PR China
[*]E-mail: ruanle@glut.edu.cn

Received: 10 January 2017 / *Accepted:* 10 November 2017 / *Published:* 28 December 2017

The triazol-3-ylamine and three different kinds of Schiff base compounds are self-assembled on bronze surface. Electrochemical impedance spectroscopy and potentiodynamic polarization measurements show that the triazol-3-ylamine and Schiff base self-assembled films can protect bronze from corrosion in 0.5 M HCl solution. The corrosion efficiency increases with the self-assembly time increasing and reaches a stable value after 8 h. The highest corrosion efficiency of the bronze electrode modified with self-assembled films reaches 95.81% after immersing in 0.005 M 2,4-Dibromo-6-[(4H-[1,2,4]Triazol-3-ylimino)-methyl]-phenol Schiff base solution for 10 h. X-ray photoelectron spectroscopy and scanning electrochemical microscope are used to characterize the inhibitive ability of the self-assembled films. Quantum chemical calculations and dynamic simulations indicate that the triazol-3-ylamine and Schiff bases molecules can absorb on the copper surface via chemisorption. The adsorption energy increases with the number of aromatic rings.

Keywords: Schiff base; bronze; inhibition; molecular simulation; XPS.

1. INTRODUCTION

Bronze, the earliest alloy in the history, has high value in the artistic, electrical conductivity and thermal work-ability [1, 2]. However bronze exposed to the pollutants which are present in the outdoor or indoor atmosphere suffer from corrosion processes which can change their appearance and stability [3, 4]. Organic compounds containing heteroatoms with high electron density such N, S, O or

those having multiple bonds which are considered as adsorption centers, are effective as corrosion inhibitors [5, 6].

Self-assembled (SA) films on copper surface have been widely used as an effective method to solve this problem, due to their hydrophobic property, and chemical adsorbed on the mental surface to prevent the Cu from corrosion in aggressive solution [7, 8]. Schiff base is a kind of compound with -=N- and -C=N- groups having lone pair electrons, easily with transition metal element outer space orbit form covalent bonds, making the self-assembled molecules easier to adsorb on the metal surface, theoretically can reduce corrosion of metal in certain circumstances [9, 10]. A new Schiff base inhibitor namely (NE)-N-(furan-2-ylmethylidene)-4-({4-[E)-(furan-2-ylmethylidene)-amino]-phenyl}-ethyl)-aniline (SB) has been synthesized by S. Issaadi et al [11]. It shown good inhibition efficiency on copper in 1 M HCl solution by electrochemical impedance spectroscopy and Tafel polarization measurements.

Table 1. The chemical structures and abbreviations of Triazol and three Schiff bases

Inhibitor name	Structure	Abbreviation
4H-[1,2,4]Triazol-3-ylamine	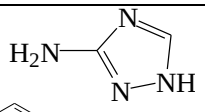	TY
2-[(4H-[1,2,4]Triazol-3-ylimino)-methyl]-phenol	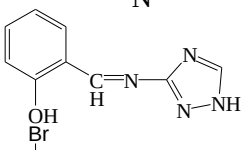	TYMP
4-Bromo-2-[(4H-[1,2,4]Triazol-3-ylimino)-methyl]-phenol	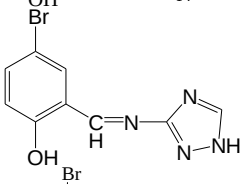	BTYMP
2,4-Dibromo-6-[(4H-[1,2,4]Triazol-3-ylimino)-methyl]-phenol	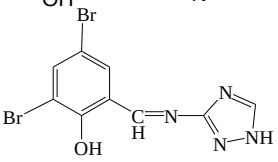	DTYMP

The aim of this paper is to investigate the inhibition performances of 4H-[1,2, 4]Triazol-3-ylamine (TY), 2-[(4H-[1,2,4]Triazol-3-ylimino)-methyl]-phenol (TYMP), 4-Bromo-2-[(4H-[1,2,4]Triazol-3-ylimino)-methyl]-phenol (BTYMP) and 2,4-Dibromo-6-[(4H-[1,2,4]Triazol-3-ylimino)-methyl]-phenol (DTYMP) SA films on bronze surface. The structures and abbreviations of all the inhibitors are listed in Table 1. Electrochemical techniques are used to study the inhibition effect of the electrode surfaces modified with different SA films in 0.5 M HCl solution.

2. EXPERIMENTAL

2.1 Materials and solution

The working electrodes were prepared from a 3.0 mm diameter bronze rod (QSn4-3, Sn-4.5%, Pb-2.0%, Zn-2.7-3.3%, Ni-0.25%, Fe-0.05%) sealed with epoxy resin. The 0.5 M HCl solution was used as the corrosion medium, which was prepared from analytical-grade HCl (12 M) and ultrapure water. All the chemical reagents and TY were purchased from Aladdin Industrial Corporation. 3-amino-1,2,4-triazole, salicylaldehyde, and 2-Bromosalicylaldehyde were used to synthesis the three kinds of Schiff base compounds [12-14].

2.2 Formation of self-assembled film

The TY and the three Schiff base compounds were dissolved in ultral water to produce the 0.005 M self-assembly solution. The cleaned electrodes were immersed in the different self-assembly solution for various immersion time at a room temperature of 25℃.

2.3 Electrochemical impedance spectroscopy (EIS) and polarization measurements

The electrochemical measurements were performed using traditional three electrodes cell with a bronze electrode as working electrode, a reference electrode-saturated electrode (SCE) and a counter electrode-platinum foil electrode. The bronze electrode was firstly polished by emery papers with different grades ($600^{\#}$, $800^{\#}$, $1000^{\#}$, $1400^{\#}$) until its surface became mirror-like bright, then it was subsequently degreased and cleaned with ethanol using an ultrasonic cleaner. The working electrodes were immersed in the TY and three Schiff bases solutions at different self-assembling times. Electrochemical measurements were performed by electrochemical workstation (CHI760E CH Instruments). The frequency range was performed from 10 kHz to 0.1 Hz, The date of impedance spectra were fitted using ZView2 software. The polarization curves were performed in a potential range of $E_{OCP} \pm 300$ mV at the scanning speed of 2 $mV \cdot s^{-1}$.

2.4 X-ray photoelectron spectroscopy (XPS) and Scanning electron microscope (SEM) measurement

Samples for XPS and SEM experiments were bronze sheets (3 mm × 3 mm × 1 mm), and the preliminary process was the same as above.

One bronze sheet was immersed firstly in the 0.005 M DTYMP solution for 12 h, then rinsed with ultrapure water and corroded in 0.5 M HCl solution for 2 h. Another bronze sheet was immersed in the 0.5 M HCl solution for 2 h. The XPS spectra were taken by ESCALAB 250 Xi system (Thermo Electron Corporation, USA). The excition source was Al Kα radiation (photoelectron energy of 1253.6 eV). Survey scans and relevant core levels were recorded: Cu 2p1/2, Br 2p/3d, N 1s, C 1s and O 1s. The results were fitted with XPS peak41 software.

After immersed in 0.005 M DTYMP solution for 12 h, the samples were corroded in 0.5 M HCl solution for 2 h. Then the bronze sheets were rinsed with ultrapure water and dried for SEM

measurements. The scanning electron microscope (JSM-6380LV) was used to observe the surface morphology on bronze surfaces without and with TY and Schiff bases films.

2.5 Quantum chemical study and molecular simulation

Quantum chemical calculation were performed using Gaussian 03 W program [15], the Lee-Yang-Parr non-local correlation functional (B3LYP) with 6-311G (d, p) basis sets was used to optimize the geometry of the inhibitor molecule [16-18]. The energies of the highest occupied molecule orbital (E_{HOMO}) and the lowest unoccupied molecular orbital (E_{LUMO}) were used to analyze the inhibition efficiency.

The molecular simulations were performed using the Materials Studio 6.0 program package from Accelrys Inc [19]. The system was utilized at 298 K, which was controlled by the Andersen thermostat, NVT ensemble, with a time step of 1.0 fs and simulation time of 1000 ps, using the COMPASS force field. Selected the most stable Cu (1 1 1) surface [20] optimized to minimum energy and enlarged to an appropriate supercell (10 × 10 × 10), the molecule dynamic simulation box was based on this supercell, including a Cu slab, a self-assembled molecule solution layer and a confined water layer. The density of the self-assembled molecule solution layer was set as 1.0 g cm^{-3}.

The simulated system included 400 H_2O molecules, 4 H_3O^+, 4 Cl^- ions and 1 self-assembled molecule. The solution layer was constructed using the Amorphous Cell molecule, and the geometry of the system was optimized such that the total energy of the system was at a local minimum with respect to potential energy. The dynamic process was carried out until the entire system, the temperature and the energy of the system reached equilibrium.

3. RESULTS AND DISCUSSIONS

3.1 Electrochemical impedance spectroscopy measurements

Fig. 1 shows the impedance spectra obtained from bare bronze electrode and bronze electrode covered with TY, TYMP, BTYMP and DTYMP SA films made with different immersion time.

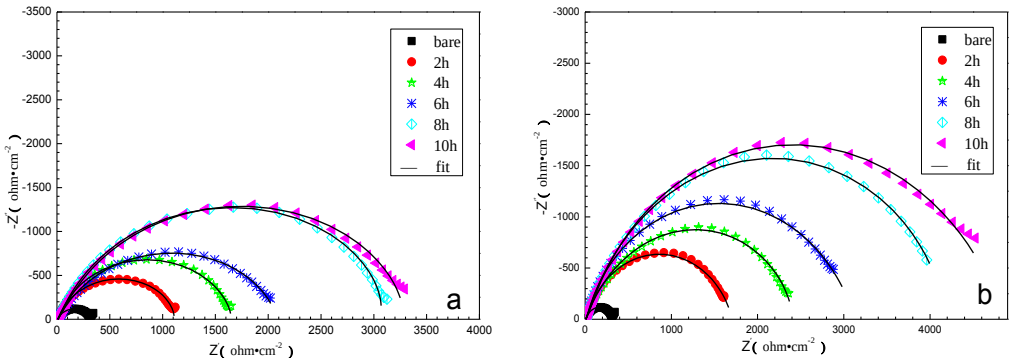

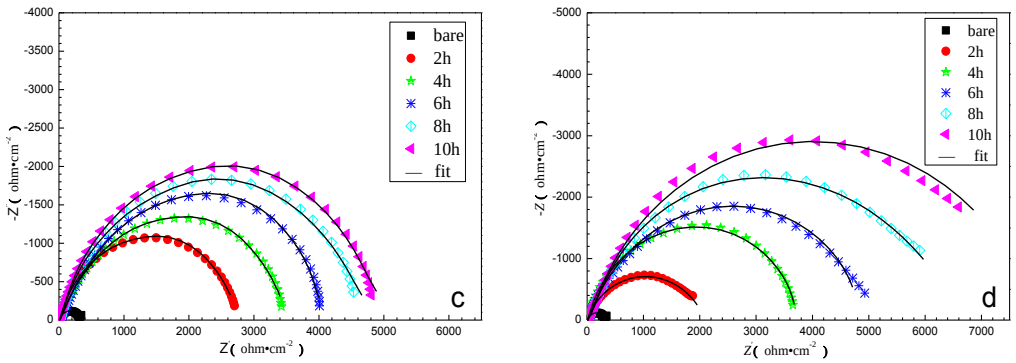

Figure 1. Nyquist impedance spectra of the bare working electrode and the working electrode covered with SA films in 0.5 M HCl solutions with different immersion time in 0.005 M TY (a), 0.005 M TYMP (b), 0.005 M BTYMP (c) and 0.005 M DTYMP (d) solutions. The solid lines are their fitted curves.

From the Nyquist impedance spectra, it can be seen that the longer assembling time, the larger diameter of semicircles. The general shape of the curves is very similar for all samples (in presence or in absence of inhibitors at different immersion times) indicating that no change in the corrosion mechanism [21]. Additionally, the semicircles are considered to be the compressed type, which is often related to the heterogeneity or roughness of ametal surface [22]. All impedance spectra are analyzed and fitted with the equivalent circuit shown in Fig. 2.

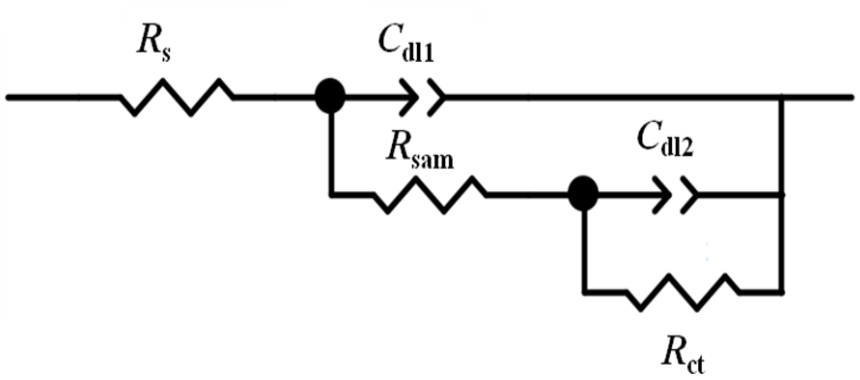

Figure 2. The equivalent circuit for fitting.

Table 2. Element value of a circuit equivalent to fit the impedance spectra in Figure 1 and the values of the protection efficiency (η) calculated by Eq. 1

Assembly molecules	Immersion time (h)	R_s (Ωcm^2)	Y_1 ($\mu\Omega^{-1}s^n cm^{-2}$)	n_1	C_{dl1}	R_{sam} (Ωcm^2)	Y_2 ($\mu\Omega^{-1}sncm^{-2}$)	n_2	C_{dl2} ($\mu F\ cm^{-2}$)	R_{ct} (Ωcm^2)	η (%)
bare	0	9.374	5.693	1.027	7.676	2.03	130.88	0.778	53.096	322.3	
TY	2	8.269	39.337	0.863	12.355	17.31	30.104	0.827	14.812	1122	71.27

	4	8.669	28.481	0.845	8.144	37.75	20.604	0.843	10.998	1655	80.53
	6	8.414	58.572	0.770	11.241	67.42	23.515	0.759	9.009	2089	84.57
	8	8.692	23.797	0.823	5.117	32.7	20.16	0.806	10.478	3252	90.09
	10	8.661	30.842	0.791	5.917	62.4	18.56	0.785	8.730	3435	90.62
	2	8.672	25.511	0.862	7.955	26.92	43.082	0.768	19.539	1688	80.91
	4	8.477	47.255	0.765	6.266	29.59	14.205	0.756	4.841	2503	87.12
TYMP	6	8.333	16.760	0.885	6.086	23.82	37.67	0.757	18.857	3088	89.56
	8	8.254	32.299	0.803	5.812	28.86	25.394	0.782	13.707	4310	92.52
	10	8.885	12.390	0.861	3.539	33.98	37.529	0.739	20.557	4864	93.37
	2	7.957	27.329	0.835	6.563	26.41	18.633	0.805	9.107	2782	88.41
	4	8.312	20.583	0.777	2.825	48.86	19.337	0.762	8.428	3648	91.17
BTYMP	6	8.698	18.296	0.769	2.567	78.42	17.315	0.783	8.445	4308	92.52
	8	8.903	14.855	0.820	2.598	23.79	21.839	0.804	12.628	4826	93.32
	10	9.207	12.589	0.836	2.655	29.22	17.586	0.827	10.617	5074	93.65
	2	8.136	23.059	0.878	7.212	10.08	72.908	0.722	35.178	2058	84.34
	4	8.337	19.454	0.856	5.432	26.34	16.397	0.833	9.389	3802	91.52
DTYMP	6	7.971	23.021	0.792	3.370	29.3	24.32	0.769	13.041	5136	93.72
	8	8.096	23.915	0.769	3.900	98.52	17.078	0.799	9.831	6481	95.03
	10	8.166	42.117	0.770	11.726	329.2	13.609	0.891	10.339	7686	95.81

In the circuit, R_s represents the solution resistance, R_{ct} represents the charge transfer resistance, R_{sam} represents the transfer resistance of electrons though the film, C_{dl1} and C_{dl2} represent two double layer capacitances corresponding to the corrosion reaction at the metal substrate/SA film and SA film/solution interface. The CPE is defined by the values of Y_0 and n is used in the model to compensate for the non-homogeneity of the electrode surface, as indicated by the depressed nature of the Nyquist semicircle [23]. The admittance and impedance of the CPE were defined as (1):

$$Y_{CPE} = Y_0(j\omega)^{-n} \text{ and } Z_{CPE} = \frac{1}{Y_0}(j\omega)^{n} \quad (1)$$

where Y_0 is modulus, j is the imaginary root, ω is the angular frequency and n is the phase. The value of n is in the range of 0.8-0.9, it often relates with the rougher of the electrode surface. The smaller the value of n, the rougher the electrode surface. The diameter of the capacitive loop increases with the assembling time, which indicates that the SA films act as good inhibitors to prevent the diffusion processes on bronze surface. The inhibition efficiency η_R can be calculated according to the equation (2) [24]:

$$\eta_R = \frac{R_{ct} - R_{ct}^0}{R_{ct}} \times 100\% \quad (2)$$

where R^0_{ct} is the charge-transfer resistance of the bare bronze electrode, R_{ct} is the charge-transfer resistance of bronze electrode modified with self-assembled films.

All the impedance data and the η values calculated by formula (2) are shown in Table 2. The value of C_{dl1} decreases with the immersing time, this is due to the replacement of the water molecules at the metal surface by the inhibitor molecules which have a lower dielectric constant. The decreasing of C_{dl2} indicates the dielectric constant decreases or the double-layer thickness increases with the immersing time. After immersing in the assembling solution for 10 h, the electrodes covered with TY, TYMP, BTYMP and DTYMP SA films reach the inhibition efficiency of 90.62%, 93.37%, 93.65% and 95.81% respectively. All the inhibitor molecules contain triazole rings which can to be adsorbed on the bronze surface by providing π-electrons to form SA films. The benzene ring -RC=N- groups in TYMP, BTYMP and DTYMP molecules facilitate the adsorbance of these groups on the bronze surface. The halogen functional groups also can increase the ability to accept electrons, so the corrosion efficiency of the SA films follows the order: TY < TYMP < BTYMP < DTYMP.

3.2 Polarization measurements

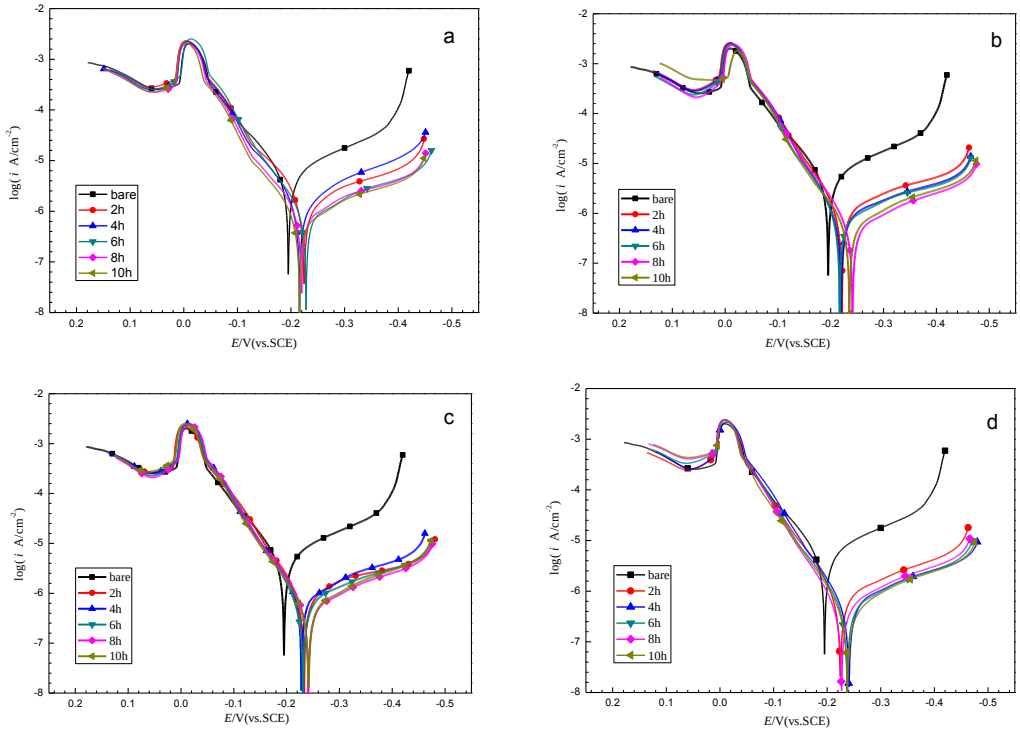

Figure 3. Polarization curves of the bare working electrode and the working electrodes covered with SA films measured in a 0.5 M HCl solution with prolonged immersion time in 0.005 M TY (a), 0.005 M TYMP (b), 0.005 M BTYMP (c) and 0.005 DTYMP (d) solutions.

Table 3. Polarization parameters for the bare-working electrode and working electrodes covered with various self-assembled films in 0.5 M HCl solution.

Assembly molecules	Immersion Time (h)	E_{corr} (V vs. SCE)	$-\beta_c$ (V dec^{-1})	βa (V dec^{-1})	i_{corr} (μAcm^{-2})	η (%)
Bare		-0.196	0.191	0.199	6.635	0.00
TY	2	-0.225	0.170	0.170	2.022	69.53
	4	-0.217	0.166	0.166	1.391	79.04
	6	-0.229	0.161	0.161	1.156	82.58
	8	-0.220	0.158	0.159	0.993	85.03
	10	-0.217	0.157	0.157	0.793	88.05
TYMP	2	-0.220	0.168	0.168	1.404	78.84
	4	-0.220	0.165	0.165	1.037	84.37
	6	-0.218	0.163	0.162	1.023	84.58
	8	-0.241	0.158	0.157	0.672	89.87
	10	-0.237	0.156	0.156	0.649	90.22
BTYMP	2	-0.234	0.168	0.168	1.205	81.84
	4	-0.229	0.161	0.161	1.156	82.58
	6	-0.232	0.162	0.162	0.770	88.39
	8	-0.241	0.159	0.151	0.670	89.90
	10	-0.241	0.156	0.156	0.607	90.85
DTYMP	2	-0.225	0.163	0.163	0.996	84.99
	4	-0.240	0.160	0.160	0.631	90.49
	6	-0.238	0.156	0.156	0.583	91.21
	8	-0.227	0.155	0.154	0.477	92.81
	10	-0.240	0.155	0.155	0.459	93.08

The polarization curves of the bare bronze electrode and the bronze electrode covered with Schiff bases SA films with different immersing time in 0.5 M HCl solution are shown in Fig. 3. It can be seen that the cathodic current densities of the bronze electrodes are reduced significantly with the immersion time prolonged, and anode curves are nearly overlap with the immersion time prokonged, its indicates that these inhibitors all acted as cathodic type inhibitor. The corrosion potential (E_{corr}) of the modified electrode reduces with the assembling time increasing. It is likely that the inhibitor modules have adsorbed onto the copper surface, and it might be difficult for the corrosion to proceed to the next step [25]. The inhibition efficiency can be calculated by the following equation Eqs. (3):

$$\eta = \frac{i^0_{corr} - i_{corr}}{i^0_{corr}} \times 100\% \quad (3)$$

where i^0_{corr} and i_{corr} represent the corrosion current densities of the bare and SA film modified bronze electrodes, respectively.

The electrochemical parameters such as the E_{corr}, cathodic and anodic Tafel slopes β_c and β_a, the corrosion current density (i_{corr}) obtained from processed polarization curves by Tafel extrap-olation and the η calculated from Eqs. (3) are shown in Table 3. The i_{corr} values of work electrodes decrease with the immersion time, which indicates the SA films on the bronze surface can protect the mental surface from corrosion. After immersing in the inhibitor solution for 10 h, the i_{corr} values of the electrodes covered with TY, TYMP, BTYMP and DTYMP SA films decrease to 0.793 μAcm^{-2}, 0.649 μAcm^{-2}, 0.607 μAcm^{-2}, 0.459 μAcm^{-2}, respectively, and the corrosion rate follows the order: TY > TYMP > BTYMP > DTYMP. These results are consistent with the EIS studies.

3.3 XPS and SEM measurements

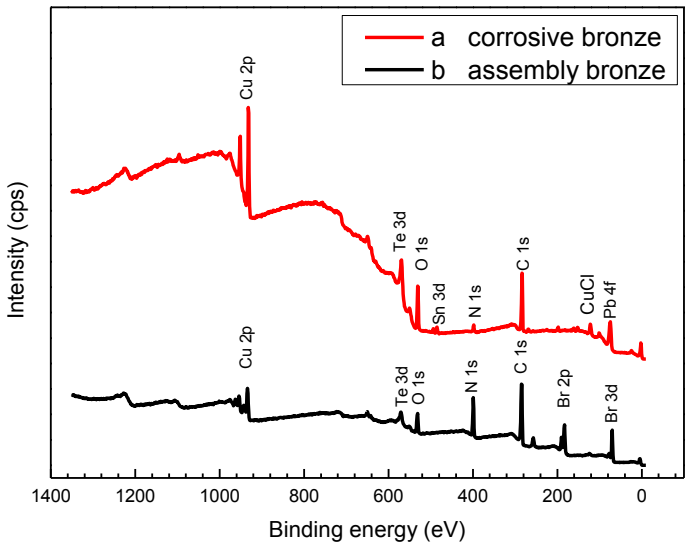

Figure 4. Wide-scan XPS spectrum of the DTYMP modified bronze surface.

The XPS spectra were used to determine the composition of the bronze surfaces covered with and without DTYMP SA films. The wide-scan XPS spectra of the two electrodes are shown in Fig. 4. The corrosive bronze shows the XPS spectra of Cu 2p, O 1s, N 1s, C 1s, Cl 1s and the SA film modified bronze shows the XPS spectra of Cu 2p, O 1s, N 1s, C 1s, Br 2p/3d. The peak of Cl 1s is due to the adsorption of chloride from the HCl solution on bronze surface.

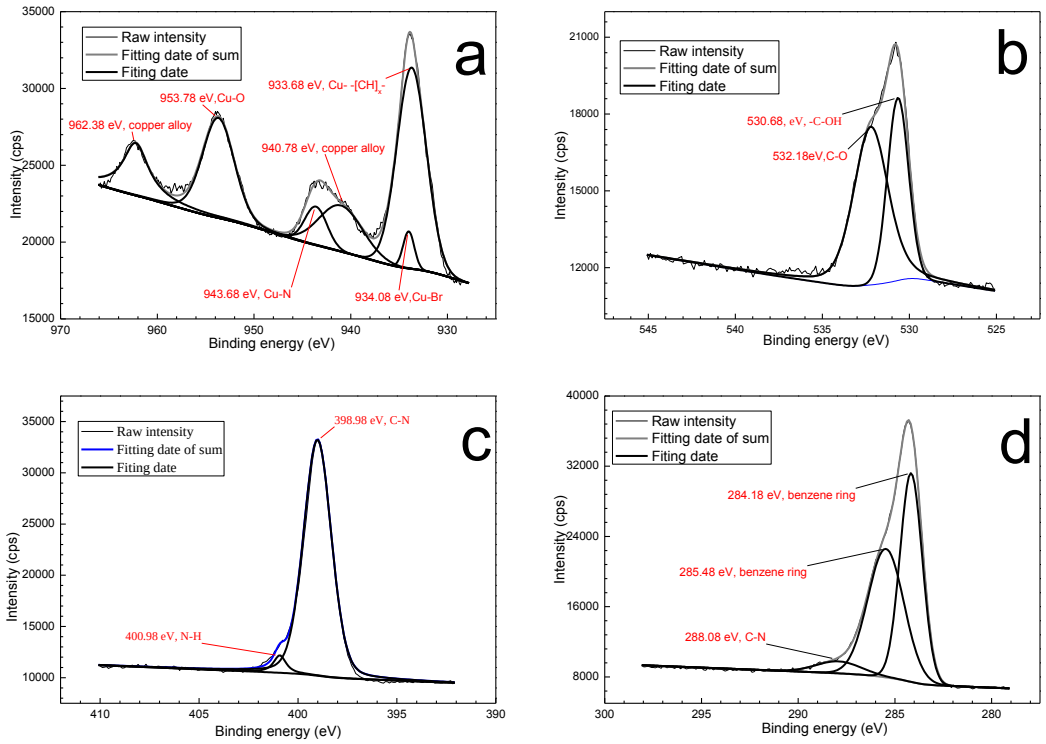

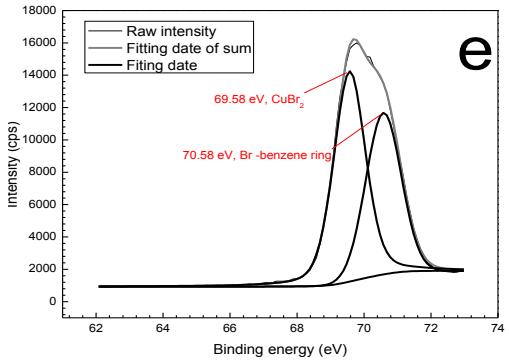

Figure 5. High-resolution XPS spectra of DTYMP modified the bronze surface: Cu 2p1/2(a), O 1s (b), N 1s(c), C 1s (d), Br 2p/3d (e).

The peak of Br 2/3d on the SA films modified bronze surface is due to the DTYMP molecules adsorbed on metal surface. The intensity of peak Cu 2p of the DTYMP modified bronze is weaker than that of the bare bronze which indicates the inhibition molecules have adsorbed on the bronze surface. Then we fitted each high-solution XPS spectrum to determine the components by checking the elements of the energy of XPS. Fig. 5 (a) shows the peaks for Cu 2p1/2 at 962.38 eV, 953.76 eV, 943.68 eV, 940.78 eV, 934.08 eV, and 933.68 eV. The composition of 962.38 eV and 940.78 eV is the copper alloy, the composition of 943.68 eV and 933.68 eV is the Cu-[CH]- from Cu-inhibitor complex, the composition of 953.78 eV may be caused by the presence of oxidation of copper on the bronze surface. The peaks of 532.18 eV and 530.68 eV shown in Fig. 5 (b) are the O 1s, mainly correspond to the oxidized copper or the inhibitor of –OH absorbed on the mental surface. Fig. 5 (c) shows the N 1s spectrum, the composition of 398.98 eV and 400.98 eV are the C-N and N-H groups from the inhibitor. The peaks of 284.18 eV and 285.48 eV in Fig. 5 (d) are the C atoms from benzene rings of inhibitor molecules. The peaks of 69.58 eV and 70.58 eV in Fig. 5 (e) indicate the Br atoms from the inhibition molecule combini with Cu. All the peaks indicate that the inhibition molecules of DTYMP are absorbed on the bronze surface that can protect the bronze from corrosion in 0.5 M HCl solution.

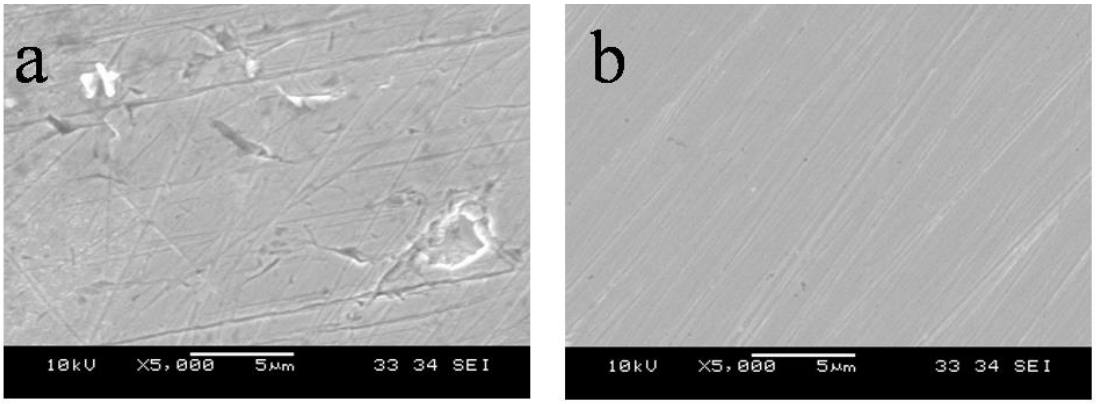

Figure 6. SEM images obtained from bronze sheets without (a) and with (b) DTYMP SA films corroded in 0.5 M HCl for 1 h.

The surfaces morphological analysis of the bronze electrodes modified without and with DTYMP SA films corroded in 0.5 M HCl for 2 h are performed by SEM. It can be seen from Fig. 6 (a) that the surface of the electrode without any protection has some small corroded holes and is not as smooth as the electrode surface covered with DTYMP SA films in Fig. 6 (b). This result confirms the absorption of the inhibitors on the bronze surface that can protect bronze from corrosion efficiently.

3.4 Theoretical study

3.4.1 Quantum chemical study

Quantum chemical study is used to further investigate the interaction between the inhibitor molecules and bronze surface. The structures of the inhibitors are optimized at the B3LYP/6-311G (d, p) level of theory in aqueous phase, the results are shown in Table 4. E_{HOMO} indicates the capacity of a molecule to donate electrons and E_{LUMO} indicates the capacity to accept electrons. E_{HOMO}, E_{LUMO}, the energy gap ($\Delta E = E_{LUMO} - E_{HOMO}$), the dipole moment ($\mu$), the absolute electronegativity (χ), the global hardness (γ), the change in the number of electrons transferred (ΔN), the adiabatic ionization potential (I, $I=E_{(optimized\ cation)}-E_{(optimized\ neutral)}$) and the adiabatic electron affinity (A) are used as the quantum chemical parameter to analyze the global reactivity of the molecules [26, 27].

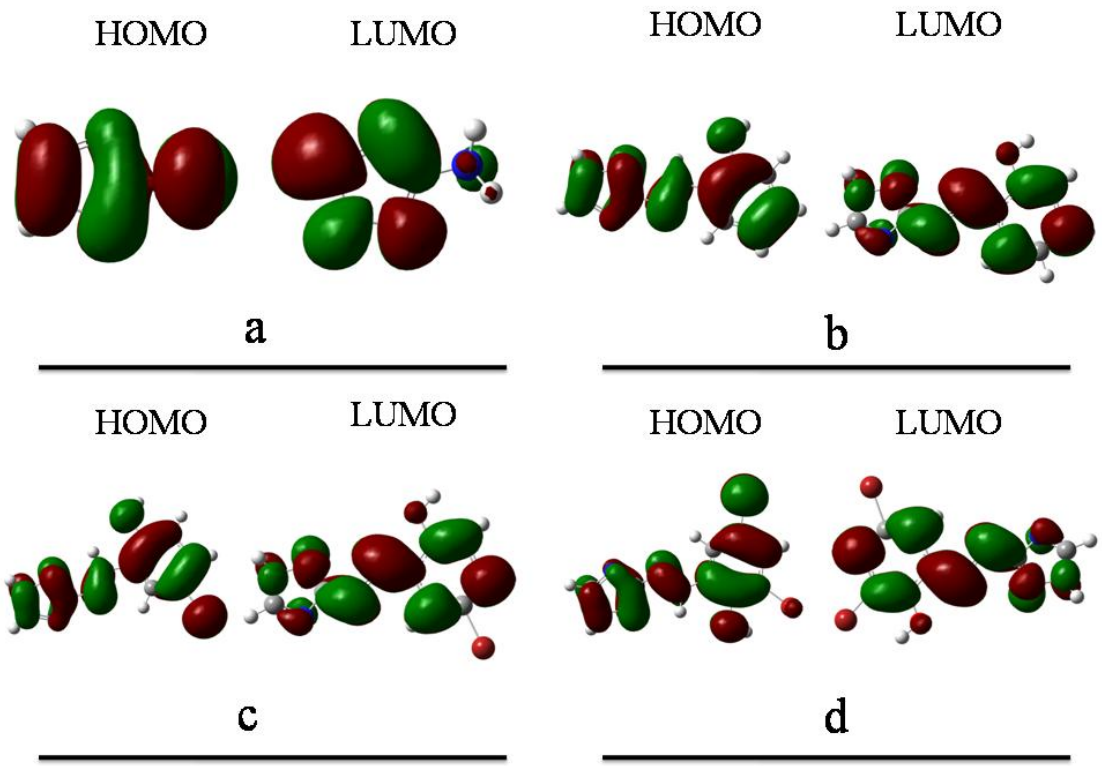

Figure 7. The HOMO and LUMO molecular orbitals TY (a), TYMP (b), BTYMP (c) and DTYMP (d).

Table 4. Quantum chemical parameters calculated using the B3LYP method with a 6-311G (d, p) basis set for Triazol and three Schiff bases molecules.

Assembly molecule	E_{HOMO} (eV)	E_{LUMO} (eV)	ΔE (eV)	μ (Debye)	χ =(I+A)/2	γ =(I-A)/2	ΔN	η_{12h} (%)
TY	-5.98	0.23	6.21	2.00	2.88	3 .10	0.26	90.62
TYMP	-6.10	-1.68	4.43	3.27	3.89	2.21	0.13	93.35
BTYMP	-6.23	-1.94	4.29	5.12	4.08	2.14	0.09	93.65
DTYMP	-6.43	-2.15	4.28	4.27	4.29	2.14	0.04	95.81

Fig. 7 shows the frontier orbital surface of the optimized inhibitor molecules. High E_{HOMO} is more likely to donate electrons to the unfilled molecule orbitals of the suitable acceptor molecule, the lower E_{LUMO} value is easier for the inhibitor to accommodate an additional negative charge from the metal surface. The adsorption energy between the inhibitors and copper surface will increase while the energy gap ΔE decreases [28, 29]. As the Table 4 shown, the ΔE follows the order: TY > TYMP > BTYMP > DTYMP which means the η % of the inhibitors follows the order: DTYMP > BTYMP > TYMP > TY. The value of E_{HOMO} follows the order: TY > TYMP > BTYMP > DTYMP and the value of E_{LUMO} follows the order: DTYMP > BTYMP > TYMP > TY. It indicates the aromatic rings and the halogen functional groups cannot improve the E_{HOMO} of the inhibitors but can increase the E_{LUMO} to improve the adsorption ability of the inhibitor. Besides, the high dipole moment (μ) suggests that the inhibitors molecule is easier to be polarized to interact with metal. This is consistent with the above experimental results [30].

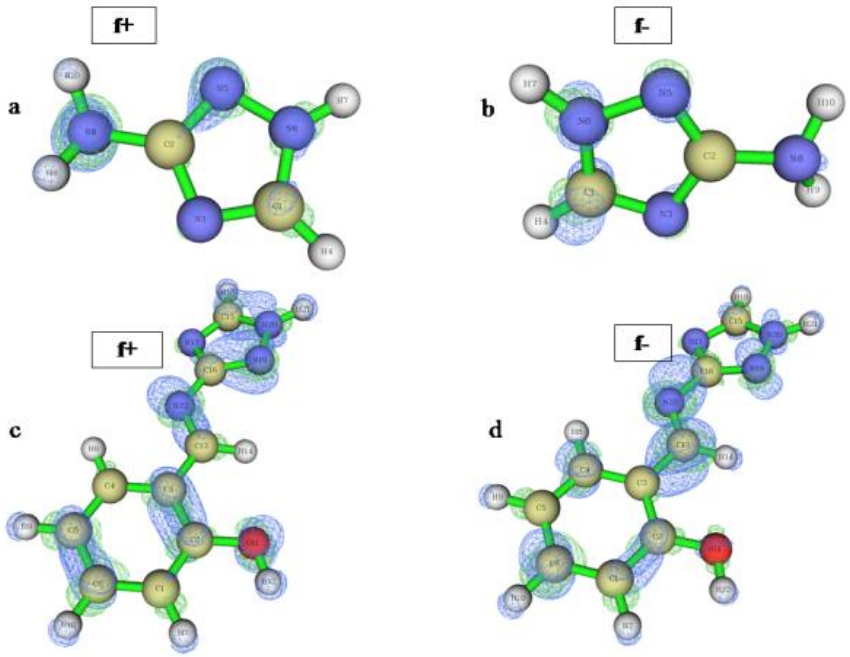

Figure 8. Fukui surface distribution of TY (a, b), TYMP (c, d), BTYMP (e, f) and DTYMP (g, h).

According to the frontier molecule orbitals (FMO), the energies of E_{HOMO} and the E_{LUMO} are related to the ionization potential (I), and the electro affinity (A) of the copper atoms and the inhibitor molecules, defined as $I = - E_{HOMO}$ and $A = - E_{LUMO}$, and the absolute electronegativity (χ), the global hardness (γ) of the inhibitor molecule are approximated by Eqs. (4) and (5):

$$\chi = \frac{I + A}{2} \quad (4)$$

$$\gamma = \frac{I - A}{2} \quad (5)$$

thus, the fraction of electrons transferred from the inhibitor to metallic surface (ΔN) is calculated by Eqs. (6) [31]:

$$\Delta N = \frac{\chi_{Fe} - \chi_{inh}}{2(\gamma_{Fe} + \gamma_{inh})} \quad (6)$$

where χ_{Cu} and γ_{Cu} are the absolute electronegativity and global hardness of the Cu atom, and the χ_{Cu} and γ_{Cu} are the absolute electronegativity and global hardness of the self-assembled molecules, respectively.

To calculate the fraction of the electrons transferred, the theoretical values of χ_{Cu} (4.48 eV) and γ_{Cu} (0 eV) are used [32], ΔN describes the ability to donate electrons to the mental surface [33, 34].

Fukui function is used to analyze the active site of the inhibitors (Fig. 8), and different substitute functional groups have different chemical behaviors. The maximum absolute values of f^+ indicates the site of a molecule that is prone to nucleophilic attack. In turn, the site for electrophilic attack is associated with the highest absolute value of f^- [35]. The selected Fukui indices with higher absolute values are shown in table 5. The Fukui functions are calculated by Eqs. (8) and (9):

$$f^+ = q_{(N+1)} - q_{(N)} \quad (7)$$

$$f^- = q_{(N)} - q_{(N-1)} \quad (8)$$

where $q_{(N+1)}$, $q_{(N)}$, and $q_{(N-1)}$ are the charges of the atoms in the systems with (N + 1), N and (N – 1) electrons, respectively.

Table 5. Selected Fukui functions of methionine and its derivatives with higher absolute values at the B3LYP/6-311G (d, p) level of theory.

TY			TYMP			BTYMP			DTYMP		
Atom	f^+	f^-	Atom	f^+	f^-	Atom	f^+	f^-	Atom	f^+	f^-
1C	-0.140	-0.267	3C	0.378	-0.219	3C	0.285	-0.255	1C	0.228	-0.238
2C	-0.301	0.378	5C	0.212	-0.010	5C	0.334	-0.125	3C	0.259	-0.268
3N	0.371	-0.374	6C	0.198	-0.336	6C	0.101	-0.262	5C	0.333	-0.138
5N	0.568	-0.436	11O	0.466	-0.369	9O	0.475	-0.366	9O	0.464	-0.344
6N	0.389	-0.405	16C	-0.293	0.294	14C	-0.278	0.304	14C	-0.276	0.311
8N	0.922	-0.446	17N	0.323	-0.320	15N	0.318	-0.319	15N	0.312	-0.318
			19N	0.400	-0.344	17N	0.336	-0.328	17N	0.333	-0.327
			22N	0.530	-0.484	20N	0.433	-0.497	20N	0.418	-0.495
						21Br	0.149	-0.025	21Br	0.132	-0.009
									22Br	0.032	-0.014

3.4.2 Molecular simulation study

The molecular dynamics was further used to investigate the interactions between the inhibitors and the Cu (1 1 1) surface. The binding energy between Cu (1 1 1) surface and the inhibitor molecules can be expressed by Eqs. (9), (10) [36, 37].

$$E_{\text{adsorption}} = E_{\text{total}} - (E_{\text{surface+solution}} + E_{\text{inhibitor+solution}}) + E_{\text{solution}} \quad (9)$$

$$E_{\text{binding}} = -E_{\text{adsorption}} \quad (10)$$

where E_{total} is the total potential energy of the system, $E_{\text{surface+solution}}$ and $E_{\text{inhibitor+solution}}$ are the potential energies of the system without the inhibitor and the system without the bronze surface, respectively. E_{solution} is the potential energy of all the water molecules. The strength of corrosion inhibitors absorbed on the copper surface can be expressed by the binding energy.

Table 6. Binding energies and inhibition efficiencies (10 h) of inhibitor molecules.

Assembly molecule	$E_{\text{adsorption}}$ (eV)	E_{binding} (eV)	$\eta_{12\text{h}}$ (%)
TY	-0.934	0.934	90.62
TYMP	-2.087	2.087	93.35
BTYMP	-2.247	2.247	93.65
DTYMP	-2.588	2.588	95.81

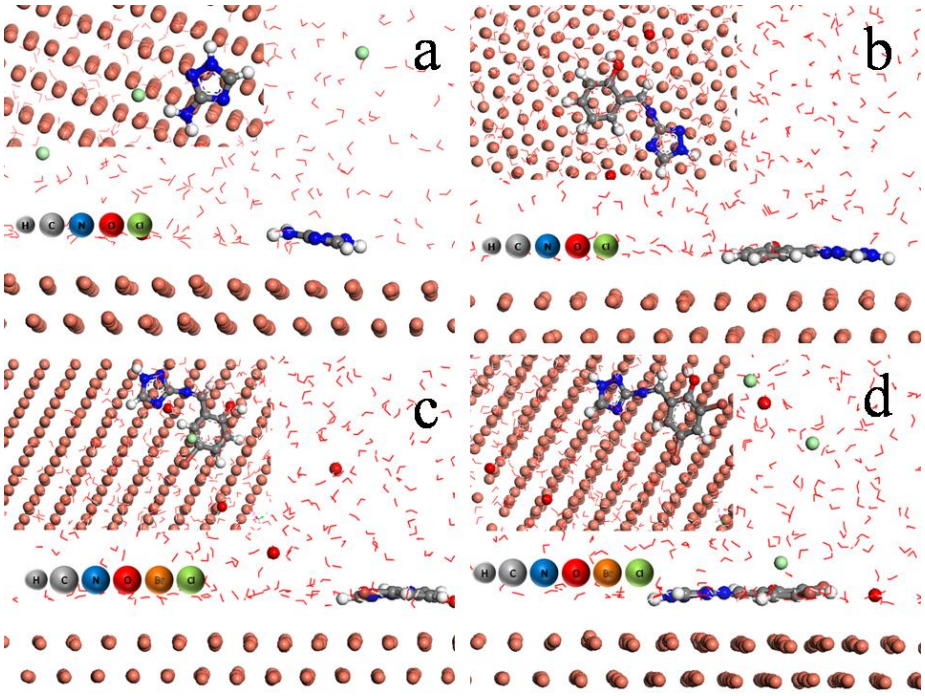

Figure 9. Equilibrium adsorption configuration of inhibitor molecules: TY (a), TYMP (b), BTYMP (c) and DTYMP (d).

Table 6 shows the potential energy of all of the water molecules and the binding energy, high value of the binding energy indicates the stronger absorbtion of inhibitors on the copper surface. The

value of the binding energy follows the order: DTYMP > BTYMP > TYMP > TY, which is consistent with the order of the corrosion efficiency. It can be inferred that the halogen functional groups can improve the accept capability by accept electrons from copper to the unoccupied π-orbital of inhibitors to form coordinate bonds, as well as by donated electrons to copper forming anti-bonding orbital coordinate bonds.

The equilibrium configuration of TY and Schiff bases adsorbed on the Cu (1 1 1) surface are shown in Fig. 9. From the top view it can be seen that all inhibitors are parallel absorbed on the copper surface. This can be explained by the five-membered ring and the aromatic rings offer the π-electrons to the unoccupied 4s-orbital of Cu to form coordinate bonds. Combining with the quantum chemical study, it can be concluded that aromatic aldehydes Schiff bases with halogen functional groups can absorb on the copper surface more closely than that without halogen functional groups because of the different donating electron ability.

4. CONCLUSIONS

Self-assembled films of triazol-3-ylamine and three Schiff bases formed on the bronze surface are investigated the inhibition effect in 0.5 M HCl solution. The inhibition efficiency increases with the immersion time prolonged, and it follows the order: DTYMP > BTYMP > TYMP > TY, which indicates the halogen functional groups of aromatic aldehydes Schiff bases can increase the adsorption capacity of the inhibitors. XPS spectra evident the chemisorption between the inhibitors and the bronze surface. SEM images detect the inhibitive ability of the SA films on bronze surface after corroded in 0.5 M HCl solution for 2 h. Quantum chemical calculations and dynamic simulations indicate that TY and three Schiff bases molecule can absorb on the copper surface via chemisorption. The halogen functional groups of the aromatic aldehydes can improve the adsorption capability on the copper surface by donating π-electrons to the unoccupied inhibitors to form coordinate bonds, as well as by donated electrons to copper forming anti-bonding orbital coordinate bonds.

ACKNOWLEDGEMENTS
This work was funded by the Nature Science Foundation of Guangxi Province of China (No. 2016GXNSFAA380061), Guangxi Key Laboratory of Electrochemical and Magnetochemical Functional Materials (EMFM20161104, EMFM20161203) and the key project of science and technology research in universities of Guangxi (2013ZD029).

References

1. G. Giovannelli, L. D'Urzo, G. Maggiulli, S. Natali, C. Pagliara, I.Sgura and B. Bozzini, *J. Solid. State. Electrochem.*, 14 (2010) 479–494.
2. R. Bostan, S. Varvara, L. Găină and L. M. Muresan, *Corros. Sci.*, 63 (2012) 275–286.
3. I. Rotaru, S. Varvara, L. Gaina and L. M. Muresan, *Appl. Surf. Sci.*, 321 (2014) 188–196.
4. T. Wang, J. Wang and Y. Wu, *Corros. Sci.*, 97 (2015) 89–99.
5. H. Jafari, I. Danaee, H. A. Eskandari and M. E. Rashvandavei, *J. Environ. Sci. Health.*, Part A 48 (2013) 1628–1641.
6. C. Liang, P. Wang, B. Wu and N. Huang, *J. Solid. State. Electrochem.*, 14 (2010) 1391-1399.
7. J. Denayer, C. Volcke, J. Delhalle and J. Mekhalif, *Electrochim. Acta.*, 63 (2012) 269–276.
8. T. Berthold, G. Benstetter, W. Frammelsberger, R. Rodríguez and M. Nafría, *Appl. Surf. Sci.*, 356

(2015) 921–926.
9. S. K. Saha, P. Ghosh, A. Hens, N. C. Murmu and P. Banerjee, *Physica. E.*, 66 (2015) 332–341.
10. Z. Quan, S. Chen, Y. Li and X. Cui, *Corros. Sci.*, 44 (2002) 703-715.
11. S. Issaadi, T. Douadi and S. Chafaa, *Appl. Surf. Sci.*, 316 (2014) 582–589.
12. K. M. Khan, S. Siddiqui, M. Saleem, M. Taha, S. M. Saad, S. Perveen and M. I. Choudhary, *Bioorgan. Med. Chem.*, 22 (2014) 6509–6514.
13. Y. M. Issa, H. B. Hassib and H. E. Abdelaal, *Spectrochim. Acta. A.*, 74 (2009) 902–910.
14. Z. H. Chohan, M. H. Anif, *Appl. Organomet. Chem.*, 25 (2011) 753 – 760.
15. M. J. Frisch, G. W. Trucks, H. B. Schlegel, G. E. Scuseria, M. A. Robb, J. R. Cheeseman, J. A. Montgomery, J. T. Vreven, K. N. Kudin, J. C. Burant, J. M. Millam, S. S. Iyengar, J. Tomasi, V. Barone, B. Mennucci, M. Cossi, G. Scalmani, N. Rega, G. A. Petersson, H. Nakatsuji, M. Hada, M. Ehara, K. Toyota, R. Fukuda, J. Hasegawa, M. Ishida, T. Nakajima, Y. Honda, O. Kitao, H. Nakai, M. Klene, X. Li, J. E. Knox, H. P. Hratchian, J. B. Cross, C. Adamo, J. Jaramillo, R. Gomperts, R. E. Stratmann, O. Yazyev, A. J. Austin, R. Cammi, C. Pomelli, J. W. Ochterski, P. Y. Ayala, K. Morokuma, G. A. Voth, P. Salvador, J. J. Dannenberg, V. G. Zakrzewski, S. Dapprich, A. D. Daniels, M. C. Strain, O. Farkas, D. K. Malick, A. D. Rabuck, K. Raghavachari, J. B. Foresman, J. V. Ortiz, Q. Cui, A. G. Baboul, S. Clifford, J. Cioslowski, B. B. Stefanov, G. Liu, A. Liashenko, P. Piskorz, I. Komaromi, R. L. Martin, D. J. Fox, T. Keith, M. A. Al-Laham, C. Y. Peng, A. Nanayakkara, M. Challacombe, P. M. W. Gill, B. Johnson, W. Chen, M. W. Wong, C. Gonzalez and J. A. Pople, Gaussian, Inc., Wallingford CT, 2004.
16. C. Lee, W. Yang and P. G. Parr, *Phys. Rev.*, 37 (1988) 785–789.
17. A. D. Becke, *J. Chem. Phys.*, 98 (1993) 5648–5652.
18. Z. Zhang, N. Tian, L. Zhang and L. Wu, *Corros. Sci.*, 98 (2015) 438–449.
19. Materials Studio, Revision 6.0, Accelrys Inc., San Diego, USA, 2011.
20. T. Qin, J. Li, H. Luo, M. Li and N. Li, *Corros. Sci.*, 53 (2011) 1072–1078.
21. Y. M. Abdallah1, Hassan. M. Hala, K.Shalabi and A.S. Fouda, *Int. J. Electrochem. Sci.*, 9 (2014)5073
22. F. Bentiss, M. Lebrini and M. Lagrenée, *Corros.Sci.*, 47 (2005) 2915–2931.
23. H. Ashassi-Sorkhabi and E. Asghari, *Electrochim. Acta.*, 54 (2008) 162–167.
24. Z. Zhang, N. Tian, X. Li, L. Zhang, L. Wu and Y. Huang, *Appli. Surf. Sci.*, 357 (2015) 845–855.
25. H. Tian, W. Li and B. Hou, *Int. J. Electrochem. Sci.*, 8 (2013) 8513–8529.
26. H. Zhao, X. Zhang, L. Ji, H. Hu and Q. Li, *Corros. Sci.*, 83 (2014) 261–271.
27. R. Yıldız, *Corros. Sci.*, 90 (2015) 544–553.
28. L. Herrag, B. Hammouti, S. Elkadiri, A. Aouniti, C. Jama, H. Vezin and F. Bentiss, *Corros. Sci.*, 52 (2010) 3042–3051
29. I. B. Obot and N. O. Obi-Egbedi, *Corros. Sci.*, 52 (2010) 198–204.
30. L. Feng, S. Zhang, S. Yan, S. Xun and S. Chen, *Int. J. Electrochem. Sci.*, 12 (2017) 1915–1928.
31. B. D. Mert, A. O. Yüce, G. Kardas and B. Yazıcı, *Corros. Sci.*, 85 (2014) 287–295.
32. N. A. Wazzan, *J. Ind. Eng. Chem.*, 26 (2015) 291–308.
33. L. Herrag, B. Hammouti, S. Elkadiri, A. Aouniti, C. Jama, H. Vezin and F. Bentiss, *Corros. Sci.*, 52 (2010) 3042–3051.
34. H. Tian, W. Li, K. Cao and B.Hou, *Corros. Sci.*, 73 (2013) 281–291.
35. X. Li, X. Xie, S. Deng and G. Du, *Corros. Sci.*, 87 (2014) 27–39.
36. A. Kühnle *Curr Opin Colloid In* 14 (2009) 157–168.
37. Z. Xu, S. Yuan, H. Yan and C. Liu, *Colloid. Surface. A: Physicochem. Eng. Aspects.*, 380 (2011) 135–142.